RELATIONAL ANALYSIS ON WEAR DIFFERENCE OF CUTTER FLANK FACE UNDER VIBRATION IN HIGH-SPEED MILLING

Minghui ZHANG[1], Bin JIANG[1], Minli ZHENG[1], and Guisheng YAO[2]
[1] *Harbin University of Science and Technology, National & Local United Engineering Laboratory of High Efficiency Cutting and Tools, Harbin 150080, Heilongjiang, China*
E-mail: mh_zhang610@hotmail.com; basuke720@163.com; fx0zmh@163. com;
[2] *Xi' an Aerospace Precision Electromechanical Institute (No.16 Institute), Xi'an 710010, Shanxi, China*
E-mail: 2792695153@qq.com

ABSTRACT*: This paper aims to analyse the wear difference of cutter flake face under vibration in high-speed mining. The cutting trajectory of the cutter tip and the tooth posture are obtained, seeking to identify the vibration-induced dynamic relationship between the friction pairs of tooth flank face. Then, the friction pair is modelled based on the vibration signals of cutter teeth captured by a high-speed camera, and the time-varying behaviour sequences are obtained. The analysis reveals that the friction contact positions of two cutters changed dynamically. Thus, the differences in the time-varying behaviour of dynamic friction are quantitatively characterized by the discrete degree and correlation analysis. The above models and methods are verified by the initial phase results of the wear experiment. This study puts forward an effective way to capture the exact time-varying features and predict the cutter wear, laying the basis for efficiency enhancement and life extension of the cutter.*
KEYWORDS*: high-speed milling cutter, wear difference, vibration, relational analysis*

1 INTRODUCTION

During milling operations, the whole milling machine is subject to a strong impact. The milling cutter vibrates under the cutting and the centrifugal forces and deviates from the original position under the periodic impact, leading to constant changes of the transient cutting state. In this case, dynamic features are observed on the friction pair between the tooth and the workpiece (Zhang et al., 2017). The time-varying behaviour of flank face friction changes with the vibration of the milling cutter, leading to the differences in the flank face friction process of each tooth (Wu et al., 2015; Tamás et al., 2016). The vibration-induced dynamic changes of flank face friction in milling cutter should be evaluated under the cutting load.

The milling cutter is bound to suffer from wear due to long-time friction (Ansari et al., 2016). Currently, the cutter wear is usually measured by the average or maximum wear width of flank surface (Mihalache & Nagit, 2016). By this method, wear feature curves can be drawn through milling cutter wear experiments, revealing the variation of flank face wear width with the cutting stroke. The tool wear standards limit the service life of the cutter (Zhang et al., 2016; Liu et al., 2001). Tambe et al. studied the friction velocity of the higher pair contact, considering the microcosmic aspect (Tambe et al. 2005). Xie et al. suggested monitoring cutter wear online by vibration signals (Xie et al., 2013; Xie et al., 2016). Based on vibration signal processing, feature analysis and diagnosis algorithms, Wang et al. put forward a method that inspects dimension error and auto-compensates tool wear online for turning operation (Wang et al., 2016). Liu et al. examined how the flank face wear of the tool is affected by the vibration features of the toolholder system in high-speed milling (Liu et al., 2008). To sum up, these studies only reflect the average tool wear of different cutting paths, but fail to disclose the dynamic features of friction wear.

In this paper, the vibration-induced tooth cutting behaviour is evaluated to simulate the dynamic friction pair of the tooth flank face, and to analyse the variation in friction pair vectors of the flank face. The simulation model can calculate the position and velocity of friction contact points. Based on the model, the time-varying behaviour sequences of flank face friction under the vibration are obtained. Then, the differences in the time-varying behaviour of dynamic friction are quantitatively characterized by the discrete degree and correlation analysis. The above models and methods are verified by the initial phase results of the wear experiment.

2 FLANK FACE FRICTION PAIR

A global coordinate system *O-xyz* is established with the origin *O* being the intersection point of the two sides and the upper surface of the workpiece, the *x*-axis along the feed direction, *y*-axis along the

cross feed direction, and *z*-axis along the axial direction of the machine tool spindle. Figure 1 shows the global coordinate system *O*-*xyz* and the local coordinate system of milling cutter O_d-*abc*.

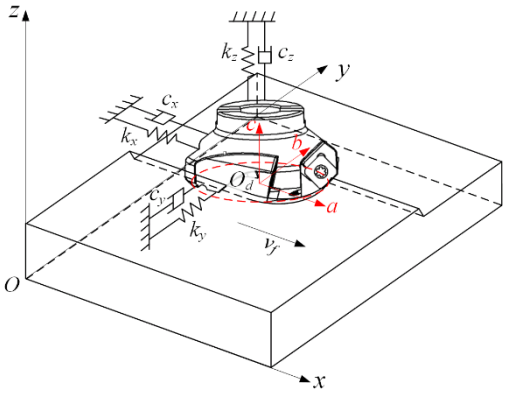

Figure 1. Milling cutter motion under vibration

where R is the cutter radius; ω is the angular velocity; φ is the initial phase angle; θ_{pi} is the angle between the ith tooth and the first tooth cutting into the workpiece; Δz_i is the axial installation error of ith tooth; v_f is the feed velocity; a_e is the cutting width; a_p is the cutting depth; s is the number of tool path intervals; Δx, Δy and Δz are the *x*-axis, *y*-axis and *z*-axis components of the vibration-induced cutter displacement, respectively.

Considering the deviation of the milling cutter, the cutter tip trajectory under vibration can be calculated by:

$$\begin{cases} x_0 = R\cos\beta\sin(\varphi+\omega t+\theta_{pi}) - \Delta z_i \sin\beta + v_f t - R + \Delta x \\ y_0 = R\sin\alpha\sin\beta\sin(\varphi+\omega t+\theta_{pi}) + R\cos\alpha\cos(\varphi+\omega t+\theta_{pi}) - \Delta z_i \sin\alpha c\cos\beta + sa_e - R + \Delta y \\ z_0 = R\cos\alpha\sin\beta\sin(\varphi+\omega t+\theta_{pi}) + R\sin\alpha\cos(\varphi+\omega t+\theta_{pi}) + \Delta z_i \cos\alpha\cos\beta + h_w - a_p + \Delta z \end{cases} \quad (1)$$

Figure 2 presents the reference point J_c at a distance of $a_p/2$ from the cutter tip on the cutting edge. The reference point can be obtained by:

$$\begin{cases} a_{iJ_c} = -\dfrac{a_p \sin\lambda_{is}}{2\sin\kappa_{ir}} \\ b_{iJ_c} = \sqrt{\left(\dfrac{a_p\cos\lambda_{is}}{2\sin\kappa_{ir}}\right)^2 - \left(\dfrac{a_p}{2}\right)^2} \\ c_{iJ_c} = \dfrac{a_p}{2} \end{cases} \quad (2)$$

The theoretical contact position between the transition surface and the flank face is set to point *J*. Then, the friction contact point of flank face under vibration in the coordinate system O_d-*abc* can be obtained by:

$$(a_{iJ}, b_{iJ}, c_{iJ}) = \left(-\frac{a_p\sin\lambda_{is}}{2\sin\kappa_{ir}} - R_n\tan\frac{\theta_r}{2}\cos\alpha_{i0}, \sqrt{\left(\frac{a_p\cos\lambda_{is}}{2\sin\kappa_{ir}}\right)^2 - \left(\frac{a_p}{2}\right)^2} - R_n\tan\frac{\theta_r}{2}\cos\gamma_{i0}, \frac{a_p}{2} \right) \quad (3)$$

where λ_{is}, κ_{ir} and γ_{i0} are the inclination angle, entering angle and rake angle of ith tooth, respectively.

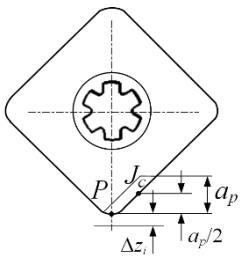

Figure 2. Reference point of cutter fiction pair

Figure 3 decomposes the cutting speed under vibration in the global coordinate system. As shown in the figure, the relative speed among the friction pairs varies with the position of tooth friction. According to the velocity component of the friction contact point on the milling plane under vibration, the velocity of friction contact point relative to the workpiece can be obtained by the equation below:

$$v_w^v = \sqrt{\begin{aligned}&(v_c\cos\theta_w^v - v_y)^2 \\ &+(v_f + v_c\sin\theta_w^v + v_x)^2 + (v_z)^2\end{aligned}} \quad (4)$$

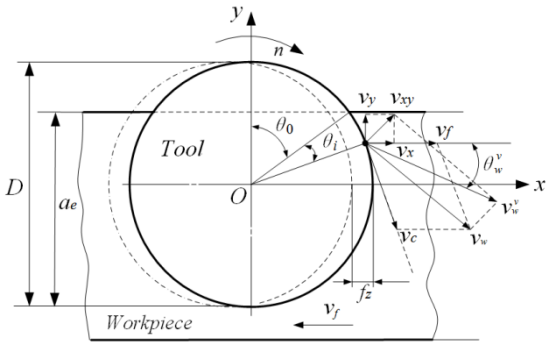

Figure 3. Decomposition of cutting speed under vibration

3 RECOGNITION AND SOLUTION OF TRANSIENT CUTTING BEHAVIOUR OF TOOTH

Figure 4 shows the five-axis CNC machining centre (Mikron UCP710). In the platform, the cutter diameter is 63mm, the cutting edge angle is 45°, the relief angle is 20°, the rake angle is 0°, and cutter

teeth are numbered clockwise. The parameters of two cutter structures are listed in Table 1. During the experiment, the cutting speed is 700m/min, the milling depth is 0.5mm, the feed per tooth is 0.15mm, the cutting width is 56mm, the cutting length is 0.5m and the workpiece material is 45# steel.

Table 1. Structure parameters of milling cutter

Tool	Distributions of cutter teeth (°)	Installation error of the tooth (mm)
Cutter A	90 90 90 90	0.013 0 0.011 0.014
Cutter B	88 89 91 92	0.012 0.009 0 0.013

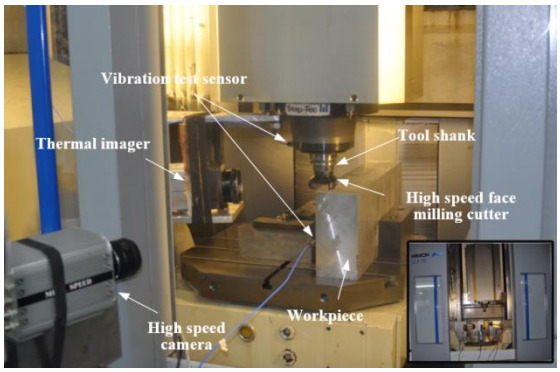

Figure 4. Five-axis CNC machining centre

During the milling process, the vibration time domain signals included cutting load signals of multiple teeth and the existing randomness on each tooth that cut into the workpiece during the initial phase. Meanwhile, there is a vague correspondence between the cutting behaviour of each tooth and the time domain vibration signals. Therefore, the cutter vibration is tested by a dynamic signal test system (DHDAS5922), which has a sampling frequency of 20kHz, analysis frequency of 7.81kHz; the cutting vibration signal is sensed by a 356A02 ICP three-axis accelerometer, whose sensitivity is 10mV/g, range is ±500g, and resolution is 0.0005g. The milling process is tracked by a high-speed camera (Mega Speed), and the real-time vibration signal is determined for each tooth (Figure 5).

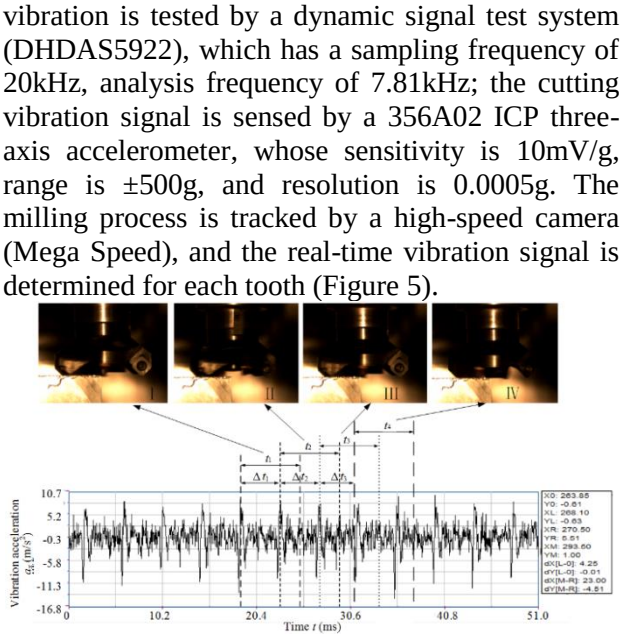

Figure 5. Real-time vibration signal of each tooth

The feature parameters of kurtoses and waveform factors are extracted to analyse the variation in the time-domain waveform of the milling cutter vibration. Then, the cutting period is determined based on the critical point in the time-domain waveform (Cosma, 2015). Figure 6 displays the time-domain waveforms extracted from the experiment in the *x*-direction and *y*-direction.

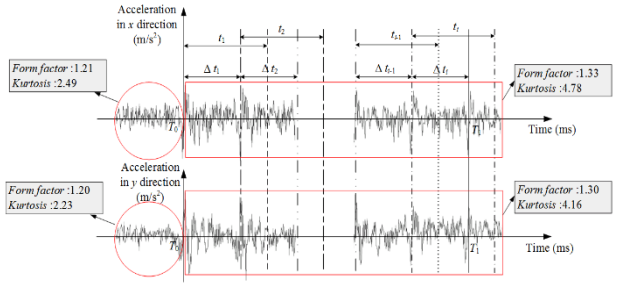

Figure 6. Cutting period of each tooth

In Figure 6, T_0 is the time the cutter enters the workpiece; T_1 is the time value of one spindle period; t_1, …, t_i (i=1, …, Z) are cutting time of each tooth in one spindle period; Δt_1, …, Δt_i are the time interval of two adjacent teeth. The relationship among these variables can be expressed as:

$$T_1 - T_0 = \Delta t_1 + \mathrm{L} \ + \Delta t_i = \frac{60}{n} (i = 1, \mathrm{K}\ , Z) \tag{5}$$

$$\Delta t_i = \frac{30 \Delta \theta_{pi}}{\pi n} (i = 1, 2, \mathrm{K}\ , Z) \tag{6}$$

According to the recognition method of transient cutting vibration signals, the last cutting-out image of each tooth is extracted from the high-speed camera to identify the corresponding vibration signal waveforms and the cutting-out time of each tooth. In this way, the author obtained the vibration information of each tooth. The results of the vibration experiment reveal the inconsistency of cutters of different tooth spacing in vibration and cutting period, and the difference in amplitude of the cutter teeth at the same cutting position. These findings evidence the difference on the cutter flank face wear under vibration.

Moreover, the high-speed and short-taper shank Hohl Shaft Kegel (HSK) tool system is introduced to the experiment. The cutter is featured by high positioning accuracy, great stiffness, small size and light weight. Because of the sufficient rigidity of the machine tool spindle, the tool shank selected to connect the cutter and form a rigid connection with the spindle. The resulting processing system, a flexible one in nature, vibrated under the cutting force. The vibration results of spindle sensor test points are directly related to the milling cutter vibration.

The vibration acceleration equations in the *x*, *y* and *z* directions can be expressed as

$$\begin{cases} a_x(t)=\sum_{i=0}^{n} A_{xi}\sin(\omega_{xi}t+\varphi_{xi})=\sum_{i=1}^{n} a_{xi}\sin\left(b_{xi}t+c_{xi}\right) \\ a_y(t)=\sum_{i=0}^{n} A_{yi}\sin(\omega_{yi}t+\varphi_{yi})=\sum_{i=1}^{n} a_{yi}\sin\left(b_{yi}t+c_{yi}\right) \\ a_z(t)=\sum_{i=0}^{n} A_{zi}\sin(\omega_{zi}t+\varphi_{zi})=\sum_{i=1}^{n} a_{zi}\sin\left(b_{zi}t+c_{zi}\right) \end{cases} \quad (7)$$

where A_{xi} , A_{yi} and A_{zi} are the maximum amplitudes in the three directions, respectively; φ_{xi} , φ_{yi} and φ_{zi} are the vibration phase angles in the three directions, respectively; ω_{xi} , ω_{yi} and ω_{zi} are the vibration angular velocities in the three directions, respectively.

In the Chapter 2, the spindle period of the milling cutter lasts 6.64ms. For the equal-pitch cutter A, the cutting time of the current tooth is 4.24ms when the next tooth cut in; for the unequal-pitch cutter B, the cutting times of the teeth are 4.322ms, 4.285ms, 4.191ms and 4.144ms, respectively, in the clockwise direction.

The features of the cutter time-domain signal obeyed the sine wave distribution. The vibration acceleration data fitting is shown in Figure 7.

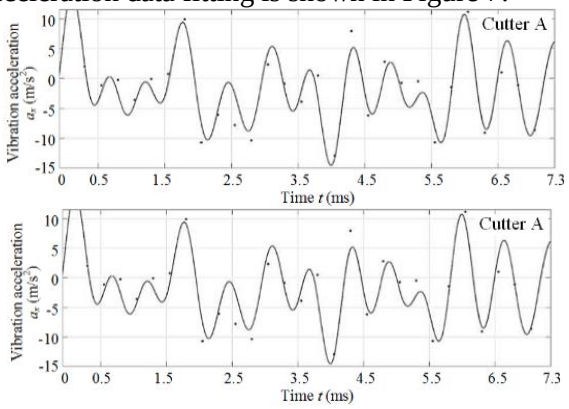

Figure 7. Vibration acceleration data fitting curves of cutters

The vibration displacement equation is obtained by double integration:

$$S_x(t)=\int_0^t\int_0^t a_x(t) \quad (8)$$

After fitting the vibration acceleration data of the cutter teeth in all directions, the vibration velocity equation and the vibration displacement equation of each tooth are processed through the integration, making it possible to obtain the transient cutting behaviour of each tooth in the initial wear phase. Then, the solving models of contact point position and relative friction pair velocity are established to describe the differences of cutter teeth under vibration.

4 WEAR DIFFERENCE ANALYSIS OF CUTTER FLANK FACE

4.1 Time-varying behaviour sequence of flank face friction under vibration

During the milling experiment, the vibration signal of the last cutting tooth in each milling cutter was extracted by vibration signal recognition and the processing. The extracted signal was substituted into the model of dynamic friction pair. Based on the position and velocity of friction contact point, the friction behaviour in the last milling period was solved and recorded in Figures 8~11 (Deshmukh et al., 2016).

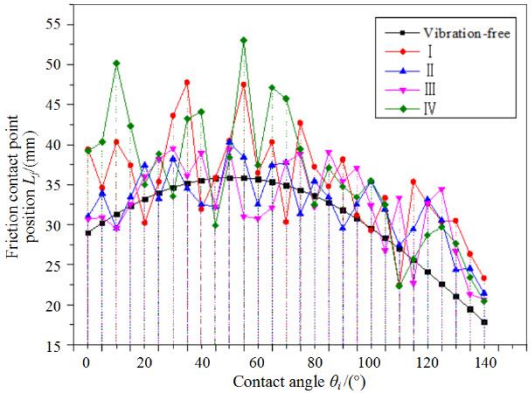

Figure 8. Solution results of friction contact position of cutter A

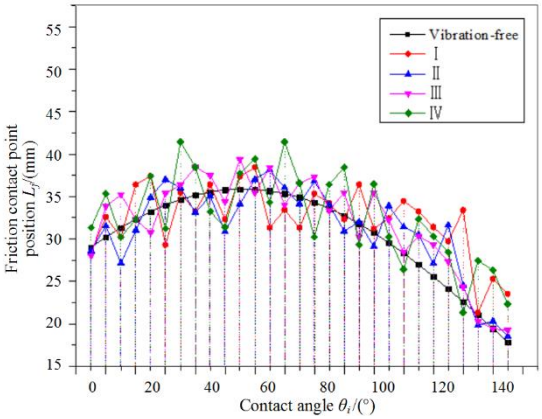

Figure 9. Solution results of friction contact position of cutter B

As shown in Figures 8~11, in the vibration-free state, the variations in the position and velocity of friction contact point in the flank face formed sine waveforms. According to the friction contact state of the flank face with different pitches under vibration, the position of friction contact point and the friction velocity of flank face are different from the initial phase; the cutting angle changed inconsistently with the transient cutting position angle in the cutting process. Under vibration, the friction pairs of the milling cutter deviated from the theoretical position, and the degree of vibration is

reflected by the ideal speed at different time and the deviation degree.

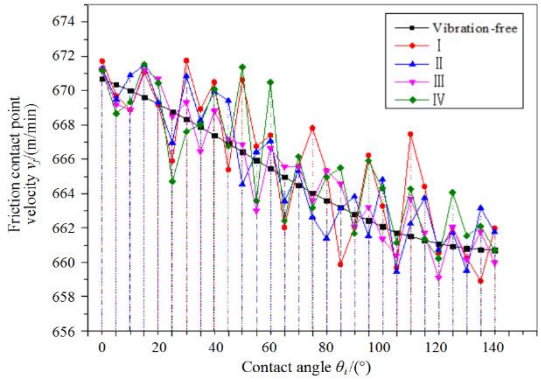

Figure 10. Solution results of friction velocity of cutter A

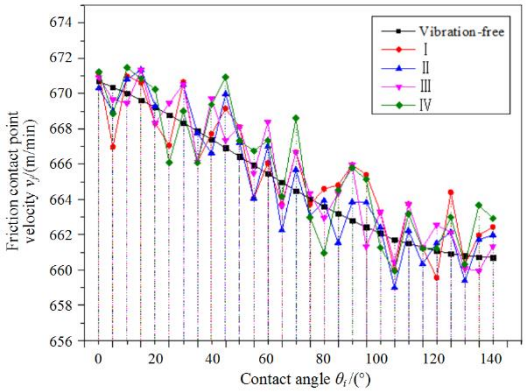

Figure 11. Solution results of friction velocity of cutter B

4.2 Relational analysis on wear difference of flank face

The discrete coefficient V is adopted to compare the discrete degree of the position and velocity of the friction contact point (Yu et al., 2011). The coefficient can be expressed as:

$$V = \frac{\sqrt{\frac{1}{N}\sum_{i=1}^{N}(x_i - \bar{x})^2}}{\bar{x}} \times 100\% \quad (9)$$

The value of the discrete coefficient is negatively correlated with the position of the friction contact point. In other words, the smaller the discrete coefficient, the more concentrated the positions of friction contact point. For equal-pitch cutter A, the discrete degrees of the position of the friction contact point are, in clockwise order, 21.61%, 14.13%, 14.73% and 24.96% from tooth I to tooth IV, and the corresponding discrete degrees of the velocity of the friction contact point are 6.08%, 5.43%, 6.18% and 6.30%. For unequal-pitch cutter B, the discrete degrees of the position of the friction contact point are, in clockwise order 13.31%, 7.91%, 8.45% and 13.22% tooth I to tooth IV, and the corresponding discrete degrees of the velocity of the friction contact point are 6.33%, 5.79%, 5.95% and 6.65%.

From the results of the discrete degrees, it is clear that the corresponding teeth of the two milling cutters differed in the wear degree of flank face. Comparatively speaking, tooth II of each of the two milling cutters is closer to the vibration-free friction state than the other teeth. For the other teeth of cutter A, the variation in the position and velocity of friction contact point is ranked as tooth III, tooth I and tooth IV in descending order; The ranking does not apply to the variation in the position and velocity of friction contact point in the other teeth of cutter B. The comparison of discrete coefficient values reveals the wear difference of each tooth and the overall wear state distribution of cutter teeth under vibration. Nevertheless, the discrete coefficient analysis only discloses the degree of deviation from the average, failing to pinpoint the exact difference of dynamiThe discrete coefficient analysis method can be generally used to evaluate the difference of the cutter tooth wear state. However, the method can only obtain the degree of deviation from the average; it cannot accurately reveal the difference of dynamic change between cutter teeth.

In order to further explore the time-varying behavior of tooth friction under vibration, the reference characteristic sequence of the position and velocity of the No. II tooth of two cutters are taken in the final cutting period, and the correlation degree of the position and speed between the No. II tooth and the other cutter teeth are shown in Tables 2 and 3 (Zhong et al., 2009; Ameur et al., 2017).

Table 2. Correlation degree between tooth II and the other teeth of cutter A

Correlation degree of the position			Correlation degree of the velocity		
$\gamma(L^v_{JAII}, L^v_{JAI})$	$\gamma(L^v_{JAII}, L^v_{JAIII})$	$\gamma(L^v_{JAII}, L^v_{JAIV})$	$\gamma(v^v_{JAII}, v^v_{JAI})$	$\gamma(v^v_{JAII}, v^v_{JAIII})$	$\gamma(v^v_{JAII}, v^v_{JAIV})$
0.720	0.826	0.714	0.806	0.893	10.787

Table 3. Correlation degree between the tooth II and the other teeth of cutter B

Correlation degree of the position			Correlation degree of the velocity		
$\gamma(L^v_{JBII}, L^v_{JBI})$	$\gamma(L^v_{JBII}, L^v_{JBIII})$	$\gamma(L^v_{JBII}, L^v_{JBIV})$	$\gamma(v^v_{JBII}, v^v_{JBI})$	$\gamma(v^v_{JBII}, v^v_{JBIII})$	$\gamma(v^v_{JBII}, v^v_{JBIV})$

0.787	0.844	0.763	0.812	0.864	0.805

Based on the nominal-the-best features in statistical theory, the cutting performance and the proximity to the ideal state depend on the closeness in positions and speeds of the friction contact points in the tooth flank face (Li et al., 2013; Jagadish et al., 2016). Hence, the increment features of the time-varying sequence of teeth friction are obtained from the absolute correlation degree ε_{ij} and relative correlation degree r_{ij}. The absolute correlation degree describes the variation in the waveform between cutter teeth, and the relative correlation degree shows the change rate of each friction contact point. The two parameters can be expressed as follows:

$$\varepsilon_{ij} = \frac{1+|s_i|+|s_j|}{1+|s_i|+|s_j|+|s_i - s_j|} \tag{10}$$

$$r_{ij} = \frac{1+|s'_i|+|s'_j|}{1+|s'_i|+|s'_j|+|s'_i - s'_j|} \tag{11}$$

$$|s_i| = \left| \sum_{k=2}^{N-1} L_{JI}^{v0}(\theta_{ik}) + \frac{1}{2} L_{JI}^{v0}(\theta_{iN}) \right| \tag{12}$$

After comparing the correlation coefficient of tooth II with that of the other teeth, the author discovered the inconsistency between the results of correlation coefficient and the results discrete degrees. This is because the changeable direction of the friction contact point under the vibration is neglected in the calculation method for discrete degree.

The results of absolute and relative correlation degrees are shown in Tables 4~7.

Table 4. Absolute correlation degree of frictional contact point position of milling cutter A

$\varepsilon(L^v_{JAI}, L^v_{JAII})$	$\varepsilon(L^v_{JAI}, L^v_{JAIII})$	$\varepsilon(L^v_{JAI}, L^v_{JAIV})$	$\varepsilon(v^v_{JAII}, v^v_{JAIII})$	$\varepsilon(v^v_{JAII}, v^v_{JAIV})$	$\varepsilon(v^v_{JAIII}, v^v_{JAIV})$
0.733	0.737	0.815	0.810	0.782	0.762
$\varepsilon(v^v_{JAI}, v^v_{JAII})$	$\varepsilon(v^v_{JAI}, v^v_{JAIII})$	$\varepsilon(v^v_{JAI}, v^v_{JAIV})$	$\varepsilon(v^v_{JAII}, v^v_{JAIII})$	$\varepsilon(v^v_{JAII}, v^v_{JAIV})$	$\varepsilon(v^v_{JAIII}, v^v_{JAIV})$
0.794	0.748	0.813	0.882	0.778	0.728

Table 5. Rrelative relation degree of frictional contact point position of milling cutter A

$r(L^v_{JAI}, L^v_{JAII})$	$r(L^v_{JAI}, L^v_{JAIII})$	$r(L^v_{JAI}, L^v_{JAIV})$	$r(v^v_{JAII}, v^v_{JAIII})$	$r(v^v_{JAII}, v^v_{JAIV})$	$r(v^v_{JAIII}, v^v_{JAIV})$
0.687	0.692	0.808	0.805	0.701	0.669
$r(v^v_{JAI}, v^v_{JAII})$	$r(v^v_{JAI}, v^v_{JAIII})$	$r(v^v_{JAI}, v^v_{JAIV})$	$r(v^v_{JAII}, v^v_{JAIII})$	$r(v^v_{JAII}, v^v_{JAIV})$	$r(v^v_{JAIII}, v^v_{JAIV})$
0.816	0.774	0.870	0.905	0.799	0.752

Table 6. Absolute correlation degree of frictional contact point position of milling cutter B

$\varepsilon(L^v_{JBI}, L^v_{JBII})$	$\varepsilon(L^v_{JBI}, L^v_{JBIII})$	$\varepsilon(L^v_{JBI}, L^v_{JBIV})$	$\varepsilon(v^v_{JBII}, v^v_{JBIII})$	$\varepsilon(v^v_{JBII}, v^v_{JBIV})$	$\varepsilon(v^v_{JBIII}, v^v_{JBIV})$
0.771	0.765	0.804	0.832	0.738	0.743
$\varepsilon(v^v_{JBI}, v^v_{JBII})$	$\varepsilon(v^v_{JBI}, v^v_{JBIII})$	$\varepsilon(v^v_{JBI}, v^v_{JBIV})$	$\varepsilon(v^v_{JBII}, v^v_{JBIII})$	$\varepsilon(v^v_{JBII}, v^v_{JBIV})$	$\varepsilon(v^v_{JBIII}, v^v_{JBIV})$
0.835	0.819	0.791	0.887	0.812	0.784

Table 7. Rrelative relation degree of frictional contact point position of milling cutter B

$r(L^v_{JBI}, L^v_{JBII})$	$r(L^v_{JBI}, L^v_{JBIII})$	$r(L^v_{JBI}, L^v_{JBIV})$	$r(v^v_{JBII}, v^v_{JBIII})$	$r(v^v_{JBII}, v^v_{JBIV})$	$r(v^v_{JBIII}, v^v_{JBIV})$
0.796	0.763	0.786	0.857	0.791	0.754
$r(v^v_{JBI}, v^v_{JBII})$	$r(v^v_{JBI}, v^v_{JBIII})$	$r(v^v_{JBI}, v^v_{JBIV})$	$r(v^v_{JBII}, v^v_{JBIII})$	$r(v^v_{JBII}, v^v_{JBIV})$	$r(v^v_{JBIII}, v^v_{JBIV})$
0.793	0.768	0.759	0.847	0.786	0.772

Similar to the flank face friction state of the two high-speed milling cutters, the relative and absolute correlation degrees of the two cutters are different in terms of the position and velocity of the friction contact point. This means the friction time-varying behaviour of the flank face exhibited obvious differences under vibration. The absolute and relative correlation degrees of the friction contact point are ranked as tooth II, tooth III, tooth I and tooth IV in ascending order in cutter A. The

absolute and relative correlation degrees of the friction contact point of each tooth in cutter B are lower than those of the corresponding tooth in cutter A, due to the relatively concentrated distribution of friction contact points of the unequal-pitch cutter under the same cutting conditions. Furthermore, the flank face of cutter B had a slower friction velocity than that cutter A, indicating that the unequal pitch can reduce vibration in the design. Despite the suppression of the unequal pitch under vibration, there is still the difference in the time-varying behaviour of the vibration and friction for the cutter teeth.

The variation in friction velocity of the contact point in the flank face is an evidence of the vibration effect. The friction velocity varied with the shift in friction contact point in the flank face. The discrete coefficients of Teeth II and III in cutter B are barely different, and the contact point speed of Tooth III is close to that of Tooth II. Furthermore, the flank face wear is a dynamic process with variable speed. The vibration brings changes to the position and the speed of the friction contact point in the flank face. Since the speed of friction contact point surpassed the theoretical value, the friction contact points shifted away from the theoretical positions, which intensified the flank face wear.

5 VERIFICATION OF WEAR DIFFERENCE OF FLANK FACE

This chapter compares the calculated results with the damage test results, aiming to verify the friction contact state model of the two milling cutters. The wear features of cutters A and B are measured by a microscope with a large depth of field (Figures 12 and 13).

According to the test results of wear width, abrasive wear is observed on the flank faces of the two milling cutters along the cutting speed direction. The abrasive wear is attributable to the microcracks, surface oxidation and roughness on the surface before cutting. It can be seen that the wear is wider on cutter A than on cutter B. In each tooth of the two cutters, the wear width ranged from 11.65μm to 5.05μm. Therefore, cutter B has a smaller range of wear width.

The above analysis confirmed that the two cutters differ in wear behaviours; the four teeth on both cutters are ranked as tooth II, tooth III, tooth I and tooth IV in ascending order of wear volume. The difference in discrete degree coincides with the difference in the initial phase position and speed of friction contact point in the flank face obtained by the model. Therefore, the solving model can reflect the exact time-varying features, and predict the cutter wear, laying the basis for efficiency enhancement and life extension.

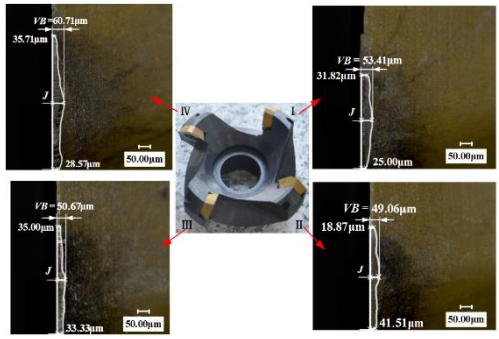

(a) Cutter A

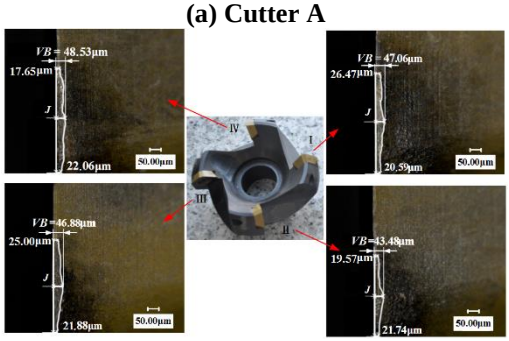

(b) Cutter B

Figure 12. Results of wear width of two cutters

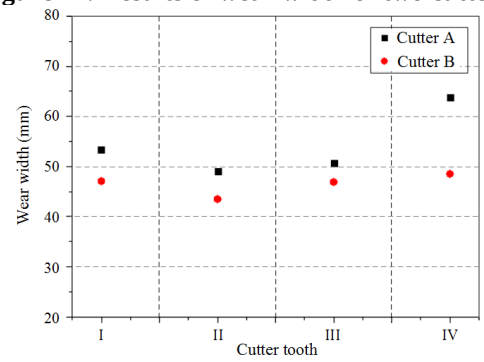

Figure 13. Measured wear width on flank faces

6 SUMMARY

In this paper, the vibration-induced tooth cutting behaviour is evaluated to simulate the dynamic friction pair of the tooth flank face, and to analyse the variation in friction pair vectors of the flank face. The simulation model can calculate the position and velocity of friction contact points. Based on the model, the author obtained the time-varying behaviour sequences of flank face friction and vibration, and acquired the time-varying behaviour sequences of flank face friction under the vibration. Then, the differences in the time-varying behaviour of dynamic friction are quantitatively characterized by the discrete degree and correlation analysis. The above models and methods are verified by the initial phase results of the wear experiment.

The research shows that there are differences in the time-varying behaviour and increment features of flank face friction under vibration; the unequal pitch cutter can effectively reduce the difference of friction for each tooth by distributing the vibration energy; the two tooth pitches resulted in different degrees of wear on the flank face. The degree of wear for each tooth coincides with the simulated and test results of the time-varying behaviour of flank face friction. The models and methods in the research can be utilized to study the evolution process of the flank face wear difference.

7 ACKNOWLEDGEMENTS

This study was supported by the National Natural Science Foundation of China under the Grant No. 51375124

8 REFERENCES

►Ameur M.F., Habak M., Kenane M., Aouici H., Cheikh M. (2017). *Machinability analysis of dry drilling of carbon/epoxy composites: cases of exit delamination and cylindricity error*. International Journal of Advanced Manufacturing Technology, 88(9-12), pp. 2557-2571.

►Ansari M.M., Chakrabarti A., Iqbal M.A. (2016). *Effects of impactor and other geometric parameters on impact behavior of FRP laminated composite plate*, Modelling, Measurement and Control A, 89(1), pp. 25-44.

►Cosma M. (2015). *Influence of tool orientation in five-axes machining process*, Academic Journal of Manufacturing Engineering, 13:(1), pp.18-23.

►Deshmukh S.V., Patil S.G. (2016). *Mathematical relationship between dependent and independent parameters of operators working on rock drill machine by dimensional analysis*, Advances in Modelling and Analysis A, 53(2), pp. 1-17.

►Jagadish, Ray A. (2016). *Optimization of process parameters of green electrical discharge machining using principal component analysis (PCA)*. International Journal of Advanced Manufacturing Technology, 87(5-8), pp. 1299-1311.

►Li S.P., Zhang E.J. (2013). *Static and dynamic robust design based on grey relational analysis*. Journal of Mechanical Engineering, 49(5), pp. 130-137.

►Liu A.M., Shen H., Kruth J.P. (2008). *Mechanism of the tool flank wear influenced by the vibration characteristics of the toolholder system in high speed milling*. Journal of Mechanical Engineering, 44(4), pp. 63-68.

►Liu Z.Q., Ai X. (2001). *Investigation of wear lifespan of cutting tools in high-speed machining*, Tool Engineering, 35(2), pp. 3-7.

►Mihalache M. A., Nagit G. (2016). *A theoretical algorithm for fea analysis and nc manufacturing*, Academic Journal of Manufacturing Engineering, 14(4), pp.86-92.

►Tamás P., Illés B. (2016). *Process improvement trends for manufacturing systems in industry 4.0*, Academic Journal of Manufacturing Engineering, 14(4), pp.119-125.

►Tambe N.S., Bhushan, B. (2005). *Friction model for the velocity dependence of nanoscale friction*, Nanotechnology, 16(10), 2309.

►Wang S.M., Chen Y.S., Lee C.Y., Yeh C.C., Wang C.C. (2016). *Methods of in-process on-machine auto-inspection of dimensional error and auto-compensation of tool wear for precision turning*, Applied Sciences, 6(4), pp. 107.

►Wu S., Liu X.L., Song S.G., Qu D. (2015). *Influence of milling cutter wear on milling stability and surface location error*. Journal of Vibration, Measurement & Diagnosis, 35(4), pp. 763-803.

►Xie H.Z., Huang M. (2013). *Research of numerical control machine tools wear monitoring method based on vibration testing*, Instrument Technique and Sensor, 2, pp. 73-75+94.

►Xie N., Ma F., Duan M.L., Li A.P. (2016). *Tool wear condition monitoring based on principal component analysis and C-support vector machine*, Journal of Tongji University (Natural Science), 44(3), pp. 434-439.

►Yu K.Z., Shi D.M., Zou H. (2011). *The random coefficient discrete-valued time series model*, Statistical Research, 28(4), pp. 106-112.

►Zhang C.L., Zhang S., Yan X.F., Zhang Q. (2016). *Effects of internal cooling channel structures on cutting forces and tool life in side milling of H13 steel under cryogenic minimum quantity lubrication condition*, International Journal of Advanced Manufacturing Technology, 83:(5-8), pp. 975-984.

►Zhang Y.T., Zhang W.M., Guo J., Guo J.Y., Guo R. (2017). *Analysis on the effects of the shapes of flexible fluid-filled containers on their impact response*, International Journal of Heat and Technology, 35(1), pp. 139-146.

►Zhong X.F., Liu S.F. (2009). *Grey relation grade for the analysis of robust designs with dynamic characteristics*. Systems Engineering-Theory & Practice, 29(9), pp. 147-152.